

First-principles studies of spin-orbital physics in pyrochlore oxides

Hiroshi Shinaoka

Department of Physics, Saitama University, 338-8570, Japan

E-mail: shinaoka@mail.saitama-u.ac.jp

Yukitoshi Motome

Department of Applied Physics, University of Tokyo, Tokyo 113-8656, Japan

Takashi Miyake

Research Center for Computational Design of Advanced Functional Materials (CD-FMat), National Institute of Advanced Industrial Science and Technology (AIST), Umezono, Tsukuba 305-8568, Japan

Shoji Ishibashi

Research Center for Computational Design of Advanced Functional Materials (CD-FMat), National Institute of Advanced Industrial Science and Technology (AIST), Umezono, Tsukuba 305-8568, Japan

Philipp Werner

Department of Physics, University of Fribourg, 1700 Fribourg, Switzerland

March 2017

Abstract. The pyrochlore oxides $A_2B_2O_7$ exhibit a complex interplay between geometrical frustration, electronic correlations, and spin-orbit coupling, due to the lattice structure and active charge, spin, and orbital degrees of freedom. Understanding the properties of these materials is a theoretical challenge, because their intricate nature depends on material-specific details and quantum many-body effects. Here we review our recent studies based on first-principles calculations and quantum many-body theories for $4d$ and $5d$ pyrochlore oxides with $B=Mo, Os,$ and Ir . In these studies, the spin-orbit coupling and local electron correlations are treated within the $LDA+U$ and $LDA+$ dynamical mean-field theory formalisms. We also discuss the technical aspects of these calculations.

1. Introduction

Electrons in solids possess not only charge but also spin and orbital degrees of freedom. Although the charge degree of freedom plays a dominant role in conventional metals and semiconductors, the situation is drastically altered in systems with strong repulsive Coulomb interactions and relativistic spin-orbit coupling (SOC). In such systems, spin and orbital are also activated and the different degrees of freedom are entangled with each other, leading to a variety of intriguing cooperative phenomena, such as metal-insulator transitions [1], unconventional superconductivity [2, 3], and cross correlation phenomena like the magnetoelectric effect [4, 5].

The pyrochlore oxides, with chemical formula $A_2B_2O_7$, provide a suitable playground to study phenomena arising from these multiple degrees of freedom. These compounds exhibit many fascinating properties which depend on the chemical constituents A and B , and on external fields like magnetic fields or pressure [6, 7]. The A and B sites are typically occupied by rare-earth and transition metal atoms, respectively. The B -site transition metal ions often play a crucial role through the multiple active degrees of freedom. In the case of $4d$ or $5d$ transition metals, such as Ru, Mo, Os, Re, and Ir, the electron interactions and the SOC can compete with each other. By changing the A -site ions, one can vary the filling of the $4d$ and $5d$ shells. This allows a systematic investigation of the keen competition between spin, charge, and orbital degrees of freedom.

Recently, first-principles calculations have attracted growing interest as a powerful tool to study such complicated systems. While the band structure calculations based on the density functional theory (DFT) [8, 9] have some difficulties in the treatment of strong electron correlations in transition-metal oxides, substantial efforts have been devoted to the development of new frameworks combining the first-principles calculations with numerical simulations based on quantum many-body theory (for a review, refer to Refs. [10, 11, 12]). To understand the diverse phenomena in the $4d$ and $5d$ pyrochlore oxides, it is obviously desired to capture the material-specific details and to take into account strong electron interactions and the SOC. This is a challenging task, but several important aspects have been unveiled by the application of the recently developed combined frameworks.

In this article, we review such theoretical efforts aimed at explaining the intriguing phenomena in $4d$ and $5d$ pyrochlore oxides, with a focus on our studies based on first-principles calculations and quantum many-body theories. We discuss how the multiple degrees of freedom of the $4d$ and $5d$ electrons bring about the various properties observed in these systems. We also elaborate on some technical aspects of the

theoretical frameworks used in these studies.

The review is structured as follows. Section 2 is devoted to a short description of the crystal structure. In section 3, after describing the general local electronic structure of $4d$ and $5d$ pyrochlores (section 3.1), we briefly review spin-orbital physics in Mo, Os, and Ir pyrochlores. More detailed discussions on Mo, Os and Ir pyrochlores are provided in sections 4, 5, and 6, respectively. In section 7 we describe the theoretical framework used in the studies reviewed in this article. A summary and future perspectives are given in section 8.

2. Crystal structure

In this section, we provide a short description of the crystal structure of the cubic pyrochlore oxides with the general formula $A_2B_2O_7$, where A is a rare earth and B is a transition metal. For different elements A and B , the cubic pyrochlore oxides exhibit a variety of physical properties. There exist several general reviews on the cubic pyrochlores [6, 7]. In particular, the magnetic properties of pyrochlore oxides were discussed in detail in Ref. [7]. As mentioned in the introduction, the pyrochlore oxides have attracted much attention in condensed matter physics since they exhibit intriguing phenomena ranging from metal-insulator transitions to geometrically frustrated magnetism and spin-orbital physics. In this section, we will explain how spin-orbital and multi-orbital physics emerges in the pyrochlores by considering their crystal structures.

The cubic pyrochlore oxides crystallize in the space group $Fd\bar{3}m$ (No. 227). Both the A and B sites form a corner-sharing network of tetrahedra. In this review, we focus on the network of B sites, where transition metal ions exhibit multi-orbital physics ‡. This network forms a pyrochlore lattice, as illustrated in Fig. 1(a). There are two kinds of tetrahedra formed by the B sites, one of which is upside-down with respect to the other one. We note that a similar pyrochlore lattice appears in the spinels AB_2O_4 as the network of the B sites.

The pyrochlore lattice is a face-centered-cubic (fcc) lattice of tetrahedra, whose primitive unit cell contains four B atoms. It can be viewed as an alternating stacking of triangular and kagome lattices along the [111] direction. In many pyrochlore oxides and related compounds, this peculiar type of corner-sharing network of transition metal ions gives rise to geometrically frustrated magnetism [7].

‡ Although our focus is on the B sites, intriguing physics arising from exchange interactions between f moments on the A sites and d electrons on the B sites has been extensively studied [13, 14, 15].

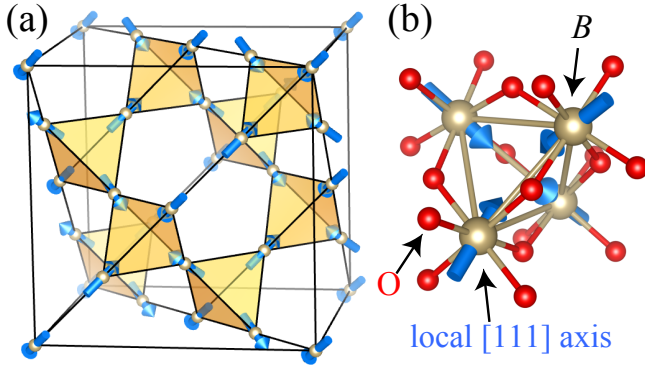


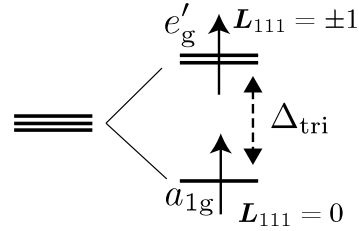
Figure 1. Crystal structure of (a) the cubic pyrochlore oxides $A_2B_2O_7$ and (b) a B tetrahedron with surrounding oxygen atoms. In (a), we only show the B atoms. The arrows indicate the local $[111]$ axes.

Let us focus on the role of the oxygen atoms in the crystal structure, since they are the source of rich orbital physics. To be precise, there are two crystallographically inequivalent positions of oxygen atoms. This is explicitly shown by writing the chemical formula $A_2B_2O_6O'$. In technical terms of crystallography, the former O sites correspond to Wyckoff position $48f$, and the O' site to $8b$. The B sites are octahedrally coordinated, being surrounded by an octahedron of six oxygen atoms in the Wyckoff position $48f$. For more details on the crystal structure, we refer to the review article by Subramanian *et al.* [6].

The octahedral coordination of the B sites plays an important role in the spin-orbital physics of the cubic pyrochlore. There is only one adjustable positional parameter for the O site in $48f$. This positional parameter is denoted by $x(O_1)$ or simply by x in the literature §. We have a perfect octahedron for $x = 0.3125$. For $x > 0.3125$, the oxygen octahedra are *compressed* along the local $[111]$ axes illustrated in Fig. 1(b). The value of x is typically in the range of 0.320–0.345 (see Sec. II A 2 of Ref. [7]). Note that the local $[111]$ axis is different for the four B sites in a unit cell. This local trigonal distortion not only lifts the degeneracy of the t_{2g} orbitals but also changes the B –O– B angle. These changes in the crystal field and bond angle may affect the electronic structure in nontrivial ways. First-principles calculations are helpful to provide insights into the electronic properties of these compounds.

§ There are several possible choices of origin for describing the crystal structure. Here, we use the convention where the B cation is chosen as the origin.

(a) Mo pyrochlores



(b) Os, Ir pyrochlores

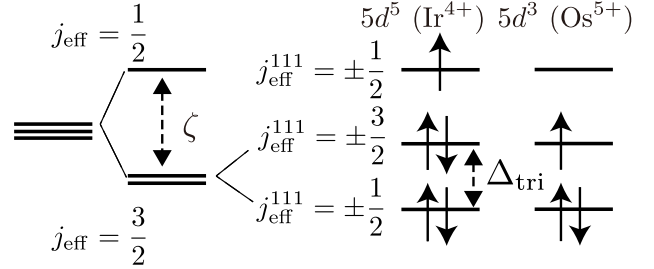


Figure 2. Crystal-field splitting of the t_{2g} orbitals for Mo pyrochlores [(a)] and Os, Ir pyrochlores [(b)]. The filling of the d shell is indicated by arrows for each compound.

3. Spin-orbital physics

3.1. Effects of crystal field and spin-orbit coupling

Figure 2 illustrates the typical crystal field splitting of $4d$ and $5d$ t_{2g} orbitals, which induces rich spin-orbital physics in pyrochlore compounds, as we are going to discuss in this review. In the pyrochlore oxides with $4d$ electrons, the effect of the trigonal crystal field Δ_{tri} is relatively large compared to the SOC ζ . Under Δ_{tri} , the t_{2g} orbitals split into doubly degenerate e'_g orbitals and a non-degenerate a_{1g} orbital, as shown in Fig. 2(a). The a_{1g} orbital is elongated along the local $[111]$ axis on each B atom [see Fig. 1(b)]. The a_{1g} and e'_g orbitals have quantized orbital momenta along the local $[111]$ axis. The splitting of the a_{1g} and e'_g orbitals for $4d$ and $5d$ pyrochlores is typically a fraction of an eV, which may be comparable to the Hund's coupling in magnitude. In $4d$ Mo pyrochlores such as $Y_2Mo_2O_7$, each Mo^{4+} ion is in a $4d^2$ electron configuration. The Hund's coupling aligns the two spins parallel as illustrated in Fig. 2(a), leaving the orbital degeneracy of the e'_g orbitals. In later sections of this review, we will see that this active orbital degree of freedom cooperates with the SOC, which results in non-trivial spin-orbital physics.

The one-particle crystal-field levels for $5d$ pyrochlores may be better understood by first considering the effect of the SOC ζ , as it is usually larger than Δ_{tri} . As shown in Fig. 2(b), the t_{2g} orbitals split into a dou-

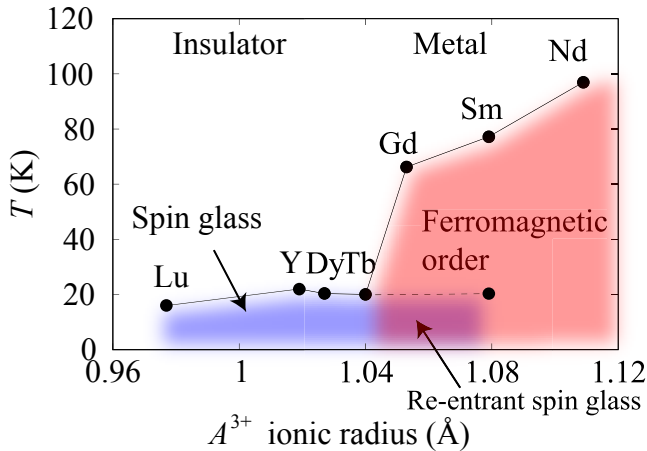


Figure 3. Experimental phase diagram of the Mo pyrochlores $A_2\text{Mo}_2\text{O}_7$. The experimental data are taken from Refs. [21, 22, 23, 24].

plet ($j_{\text{eff}} = 1/2$) and a quartet ($j_{\text{eff}} = 3/2$) by ζ . Here, the effective total angular momentum $\hat{j}_{\text{eff}} \equiv \hat{L} - \hat{S}$ is quantized [16, 17, 18]. The trigonal crystal field Δ_{tri} splits this quartet state further into two doublets, as shown in Fig. 2(b). In this case, \hat{j}_{eff} is no longer a good quantum number, but its projection onto the local [111] axis (referred as j_{eff}^{111} later) still remains quantized. For convenience, we denote these states as “ $j_{\text{eff}} = 1/2$ ” and “ $j_{\text{eff}} = 3/2$ ” states.

Pyrochlore iridates are characterized by a $5d^5$ electron configuration. In these compounds, based on the simple one-particle picture mentioned above, the $j_{\text{eff}} = 3/2$ quartet is fully filled, leaving the $j_{\text{eff}}=1/2$ state half filled. As a consequence, the properties of the pyrochlore iridates are often discussed based on an effective single-band model for the $j_{\text{eff}}=1/2$ state. On the other hand, such a simple single-band picture cannot be applied to the Os pyrochlores with a $5d^3$ configuration, as discussed in section 5.

In the above arguments, we assumed the t_{2g} orbitals to be described by Wannier functions hybridized with oxygen orbitals. In some of the literature [19], the local electronic structure was discussed in terms of atomic-orbital-like t_{2g} orbitals, which causes some confusion about the definition of Δ_{tri} . In the present convention, the effects of $B-O$ hybridizations are included in Δ_{tri} in addition to the effects of longer-range ligand fields from the A sites. The same convention of Δ_{tri} as in this review is used in the analysis in the supplemental material of Ref. [20]. The above-mentioned effects are however not included in the case of the atomic-orbital-like basis.

3.2. Mo pyrochlores $A_2\text{Mo}_2\text{O}_7$

Let us discuss several key properties of each compound in more depth. The Mo pyrochlores $A_2\text{Mo}_2\text{O}_7$ host

various interesting phenomena like metal-insulator transitions. Figure 3 shows an experimental phase diagram with respect to the A -site ionic radius and temperature. Compounds with relatively large A -site ionic radii ($A=\text{Nd}, \text{Sm}$) are metallic and exhibit a ferromagnetic transition at low T . In a previous LDA+ U study [25] it was proposed that the ferromagnetism is due to the double exchange mechanism. The essential idea is that the a_{1g} band is narrower than the e'_g band, so that the corresponding electrons act as localized spins. The relatively broader e'_g band can host itinerant electrons, leading to the double-exchange mechanism. For smaller A -site ionic radii, the ferromagnetic transition temperature decreases monotonically, and at the same time, the temperature dependence of the DC resistivity becomes insulating in the high-temperature paramagnetic phase. Some compounds with small ionic radii ($A=\text{Y}$ *et al.*) show insulating transport properties at room temperature.

One interesting phenomenon, which is commonly observed in these insulating compounds, is spin-glass behavior at low T . A spin glass is a magnetic state in which spins are frozen in random directions without spatial periodicity. Conventional spin glasses have been observed in dilute magnetic systems where the magnetic exchange couplings alternate randomly in sign [26]. However, it is believed that Mo pyrochlores are not dirty enough to host such a conventional spin glass.¶ Several experimental results indicated that there is a re-entrant spin-glass phase on the metallic side [28, 29, 24]. A fundamental question thus is what causes this apparently unconventional spin-glass state. The geometrical frustration is a possible key element. To be more specific, geometrical frustration induces competition between different magnetic states, which may somehow lead to the freezing of spins in random directions. Thus, many theoretical studies have focused on the roles of the spin degree of freedom [30, 31, 32, 33].

On the other hand, a previous first-principles study [25] already revealed the importance of the orbital degree of freedom. Solovyev performed first-principles calculations (including the SOC) and studied magnetic ordering and metal-insulator transitions in these compounds. It was revealed that in a magnetically ordered insulating state both the spin and orbital moments are active and oriented in an anti-parallel alignment. This clearly indicates the importance of the SOC and the resultant spin-orbital composite degree of freedom.

The role of the orbital degree of freedom in

|| Recent experimental results are reviewed in section III. B of Ref. [7].

¶ Refer to Ref. [27] and discussions in section III.B.1 of Ref. [7].

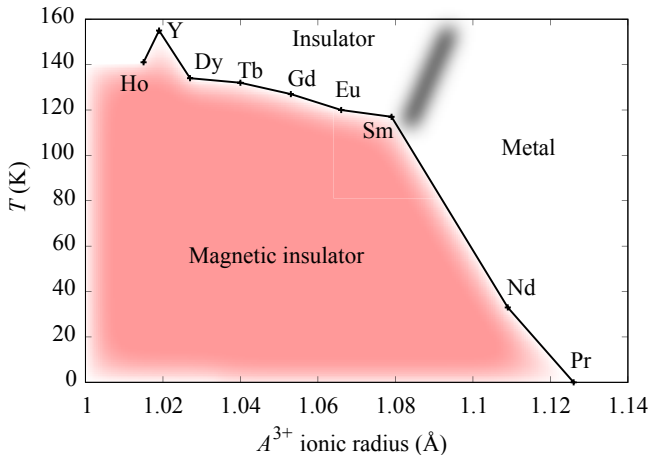


Figure 4. Experimental phase diagram of the pyrochlore iridates $A_2\text{Ir}_2\text{O}_7$. The experimental data are from Refs. [36, 37].

the spin-glass phenomena was not studied in more depth until the recent report of the first neutron scattering experimental results for single crystals of $\text{Y}_2\text{Mo}_2\text{O}_7$ [34]. A surprising observation was that the measured spin structure factor is not consistent with the conventional picture of geometrical frustration based on antiferromagnetic spin models. This experimental finding motivated some of the authors to investigate the role of orbitals and the SOC in more depth [35]. In section 4, we describe how the orbital degree of freedom and the SOC give rise to a non-trivial magnetic frustration in the Mo pyrochlores.

3.3. $\text{Cd}_2\text{Os}_2\text{O}_7$

In the Os and Ir pyrochlores, different numbers of electrons occupy the $5d$ t_{2g} orbitals, although both compounds are known to exhibit metal-insulator transitions as T is changed. The electronic properties of $\text{Cd}_2\text{Os}_2\text{O}_7$ with a $5t_{2g}^3$ configuration were reported for the first time in 1974 [38]. It was revealed that the temperature dependence of the DC resistivity becomes insulating below ~ 227 K and that a cusp appears in the magnetic susceptibility at the same T [38]. These indicate that the metal-insulator transition is associated with some magnetic ordering. There have been many experimental and theoretical studies on the origin of the transition since the first report [39, 40, 41, 42, 43, 44]. However, Cadmium has a high neutron absorption cross-section, which prevents the use of neutron scattering techniques for determining the magnetic structure. In 2012, Yamaura *et al.* reported the results of X-ray diffraction and Raman scattering experiments [45]. They revealed the existence of the all-in-all-out magnetic order below the transition temperature. In section 5, we investigate

the magnetic and electronic properties of the low- T phase using first-principles calculations [46].

3.4. $A_2\text{Ir}_2\text{O}_7$ (A =rare earth)

Figure 4 shows a phase diagram summarizing recent experimental data of $A_2\text{Ir}_2\text{O}_7$ with a $5d^5$ configuration with respect to the A -site ionic radii and temperature. In the early 2000s, the existence of metal-insulator and antiferromagnetic transitions was experimentally revealed [47, 48]. However, natural isotopes of iridium are also known as strong neutron absorbers, which has prevented the experimental investigation of the magnetic structure of the low- T phases.

The low- T properties of pyrochlore iridates have attracted much attention since a Weyl semimetal with nontrivial magneto-electric properties was proposed for the ground states of some compounds in this series in 2011 [49]. On the basis of LDA+ U calculations it has been argued that (i) some compounds are magnetically ordered in the so-called all-in-all-out structure, and (ii) there exists a Weyl semimetal phase with the all-in-all-out order in the vicinity of an insulating phase. Indeed, the all-in-all-out magnetic order has been confirmed in some pyrochlore iridates later by experiments (A =Nd, Eu) [50, 51, 52]. In recent years, angle-resolved photoemission spectroscopy (ARPES) [53] and THz optical conductivity [54] have been used to elucidate the nature of the low- T phase. As we will see later, however, the Weyl semimetal phase is absent in the LDA+dynamical mean-field (DMFT) phase diagram.

The pyrochlore iridates shown in Fig. 4 contain Ir^{4+} with a $5d^5$ configuration. In the single-particle picture, this leaves one hole in the $j_{\text{eff}}=1/2$ band as discussed in section 3.1. Thus, the electronic properties of the compounds are often discussed based on an effective single-band picture of the $j_{\text{eff}}=1/2$ orbital. However, to what extent is this simplified description justified in a quantitative study of the properties of the iridates? We discuss this point in this review based on the results of first-principles calculations performed by some of the authors and their co-workers [55]. Our particular focus will be on $\text{Y}_2\text{Ir}_2\text{O}_7$, which is located in the insulating regime. Y^{3+} has no f moment, which may make $\text{Y}_2\text{Ir}_2\text{O}_7$ a prototype compound for studying strong correlations among $5d$ electrons. In section 6, we discuss the experimental phase diagram based on a theoretical phase diagram obtained by LDA+dynamical mean field theory (LDA+DMFT) with respect to the onsite Coulomb interaction U and temperature T [55].

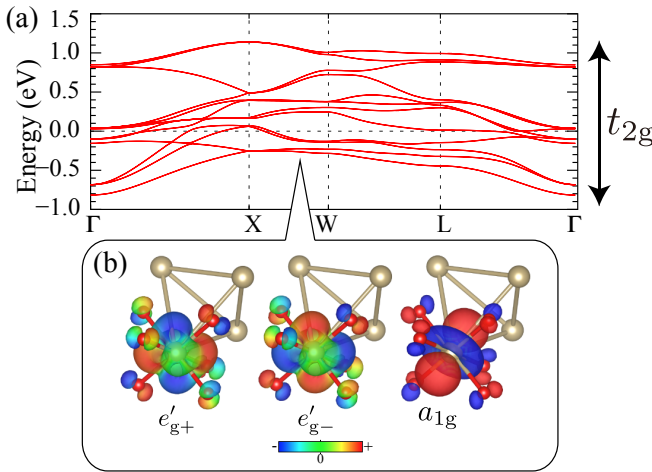


Figure 5. (a) LDA band structure computed for $\text{Y}_2\text{Mo}_2\text{O}_7$ and (b) maximally localized Wannier functions constructed from the band structure. There are twelve t_{2g} bands in (a) (each of them is doubly degenerate due to time-reversal symmetry and inversion symmetry).

4. Spin-orbital interplay in frustrated Mo pyrochlores

Figure 5(a) shows the LDA band structure of $\text{Y}_2\text{Mo}_2\text{O}_7$ in the nonmagnetic state. The effects of the SOC were included by solving the relativistic Kohn-Sham equation (see section 7). Isolated states having t_{2g} character are observed in the vicinity of the Fermi level. The nonmagnetic metallic state is stable in the LDA calculation, which is inconsistent with the insulating nature of the compound. This can be ascribed to the LDA, which underestimates electron-electron interaction effects. Solovyev studied the effect of the intra-atomic Coulomb repulsion (Hubbard U) on the Mo sites using the LDA+ U method, and showed that the effect of U makes the system insulating [25]. A Mo^{4+} ion has an electron configuration of $4t_{2g}^2$. One electron occupies the a_{1g} state which is half-filled, and the other occupies the e'_g states [Fig. 2(a)]. As the e'_g states are quarter-filled, one may expect that orbital degrees of freedom are active. However, the orbital magnetic moment of the e'_g states couples to the spin moment through the SOC ζ , and therefore they do not behave independently. In what follows, we will see that the orbital degrees of freedom of Mo^{4+} and the spin-orbital physics arising from them play a crucial role in the magnetism of this compound.

Some of the authors performed LDA+ U calculations with $U \geq 3$ eV and compared the total energy of the insulating states with different periodic magnetic structures [35]. It was found that three magnetic structures, shown in Fig. 6, are nearly degenerate in energy. In these structures, the magnetic moments are localized mostly on the Mo sites, while the O sites con-

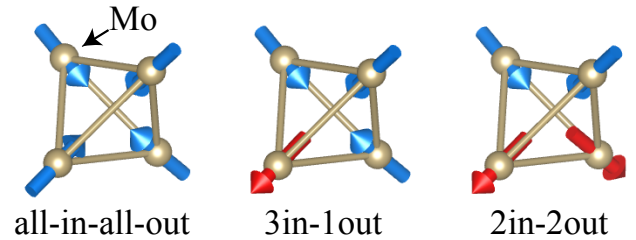


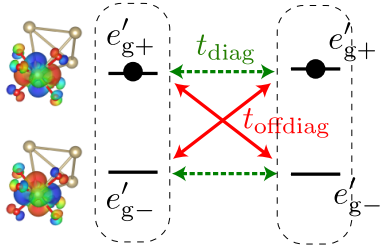
Figure 6. Three competing magnetic structures in $\text{Y}_2\text{Mo}_2\text{O}_7$.

tribute only a few percent to the spin moments. The three states are different, as the sum of the four spins at the corners of a tetrahedron is different: The all-in-all-out structure is an antiferromagnetic state where the four spin moments cancel each other, whereas the spin moments do not cancel in the other two configurations. Therefore, ferromagnetic and antiferromagnetic correlations are competing in the present system. A detailed analysis using an effective spin model and a multi-orbital Hubbard model revealed that there is keen competition between the 2in-2out and all-in-all-out magnetically ordered states. We refer the interested readers to Ref. [35] for more details. We also note that another independent DFT+ U study revealed a substantial coupling between spin and orbital degrees of freedom [34]. It was also shown that each of these orbital states is accompanied by local lattice distortions, indicating a coupling between lattice and orbital degrees of freedom.

What is the origin of this magnetic competition? As a matter of fact, it is deeply connected to the orbital degrees of freedom which have not been considered thus far. This is schematically explained in Fig. 7. Let us consider the hopping of e'_g electrons between two neighboring Mo atoms. A ferro-orbital alignment of the two electrons leads to a gain of kinetic energy when the orbital off-diagonal transfer integral t_{offdiag} dominates the orbital-diagonal transfer integral t_{diag} . In contrast, the antiferro-orbital alignment is favored in the opposite limit, namely when $|t_{\text{offdiag}}| \ll |t_{\text{diag}}|$ holds. In the case of ferro-orbital alignment, all the orbital magnetic moments on a tetrahedron are inward- or outward-oriented. Since the spin and orbital moments are antiparallel coupled by the SOC, the ferro-orbital alignment favors all-in-all-out magnetic ordering, whereas the antiferro-orbital alignment favors 2in-2out magnetic ordering.

In order to see whether t_{offdiag} or t_{diag} is dominant in the real material, some of the authors evaluated the transfer integrals between the maximally localized Wannier functions constructed from the LDA solutions [Fig. 5(b)]. It was found that the two terms are close in magnitude. This indicates that ferro- and antiferro-orbital alignments are competing in the present system,

(a) Transfers between nearest Mo atoms



(b) Ferro-orbital correlation Antiferro-orbital correlation

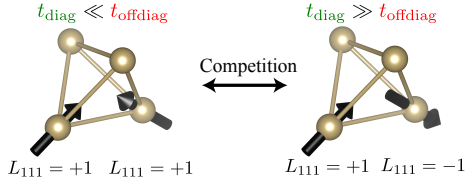


Figure 7. Competing orbital orderings in $\text{Y}_2\text{Mo}_2\text{O}_7$. (a) Hopping between e'_g orbitals. (b) Two different patterns of orbital ordering are stabilized by changing the ratio $t_{\text{offdiag}}/t_{\text{diag}}$.

which results in a competition between spin structures through the SOC.

The nature of the spin-glass phase and the role of randomness still remain to be clarified. Recently, Thygesen and co-workers performed a detailed neutron and x-ray pair-distribution function analysis of the crystal structure of $\text{Y}_2\text{Mo}_2\text{O}_7$ [56]. They found that the Mo^{4+} ions displace according to a local 2in–2out rule on each Mo tetrahedron. This indicates the important role of spin-lattice coupling and that local 2in–2out magnetic structures survive in the spin-glass phase (see Fig. 7). Long-range ordering may be prevented by the microscopic degeneracy of coverings on the pyrochlore lattice with 2in–2out structures (spin-ice-like degeneracy). Further theoretical and experimental studies are needed to settle this issue.

5. Non-collinear magnetism in Os pyrochlore

In Fig. 8, the band structures of $\text{Cd}_2\text{Os}_2\text{O}_7$ computed by the LDA+ U method are shown. The present result for $U = 0$ (corresponding to the LDA) is in good agreement with the previous result reported by Harima [41]. Since a unit cell contains four Os atoms, there are 24 t_{2g} bands (taking the spin degeneracy into account). Contrary to the Ir oxide case, to be described below, the splitting into $j_{\text{eff}} = 1/2$ and $3/2$ bands is not clearly observed. In this $5d^3$ situation, the t_{2g} bands are half occupied and semi-metal-like features are observed. When applying “+ U ” similarly to the Mo oxide case, the all-in-all-out magnetic order becomes stable as the ground state for $U \geq 0.9$ eV. It should be noted that no Brillouin-zone folding occurs

since the all-in-all-out magnetic order has a wave vector $\mathbf{Q} = 0$. As the magnetic moment grows for larger U , a small indirect gap opens between the valence and conduction bands as a consequence of the band shift induced by the magnetic ordering. At each \mathbf{k} , however, a larger direct gap exists. These features are consistent with the distinct gap observed by optical conductivity measurements [40] and the small gap deduced from the temperature dependence of the resistivity [38, 39].

In the real material, a metal-to-insulator transition occurs as T is lowered. Although the LDA+ U calculations were carried out at $T = 0$, they might give some insight into the nature of the finite- T transition. The finite- T transition may be caused by shifts of the bands when the magnetic moment increases continuously with decreasing temperature below T_c . Such a transition is called “Lifshitz transition”.⁺ A recent optical spectroscopy experiment supports this scenario [57].

In $\text{Cd}_2\text{Os}_2\text{O}_7$, the all-in-all-out magnetic order is stabilized by the strong magnetic anisotropy induced by the SOC [46]. Table 1 shows the values of the nearest-neighbor exchange coupling (J), the single-ion anisotropy (A_{sia}) and the Dzyaloshinskii-Moriya (DM) interaction (A_{DM}) estimated by LDA+ U calculations. The exact form of the effective spin model is given by Eq. (1) in Ref. [46]. There exists a strong magnetic anisotropy in this compound even near the metal-insulator transition: $A_{\text{sia}} > 0$ corresponds to an easy-axis anisotropy, while $A_{\text{DM}} > 0$ stabilizes the all-in-all-out order in combination with the antiferromagnetic $J (> 0)$.

Our LDA+ U studies were done around 2012. In those days, it was technically difficult to perform finite-temperature calculations. As described in the next section, finite-temperature calculations including electron correlation effects have in the meantime become possible even for $5d$ transition-metal oxides using the LDA+DMFT method. In parallel with the improvement of experimental techniques such as angle-resolved photoemission spectroscopy (ARPES) [53], modern first-principles calculations initiate a new era in the study of finite-temperature phase transitions. Do quasi-particle bands survive close to T_c ? What is the effect of thermal fluctuations of the magnetic moment? It is expected that these and related questions will be solved in the near future. Understanding the bulk properties of $\text{Cd}_2\text{Os}_2\text{O}_7$ is still a hot research subject [58, 57, 59, 60].

⁺ Strictly speaking, a Lifshitz transition can be defined only at $T = 0$, where the Fermi surfaces are well defined.

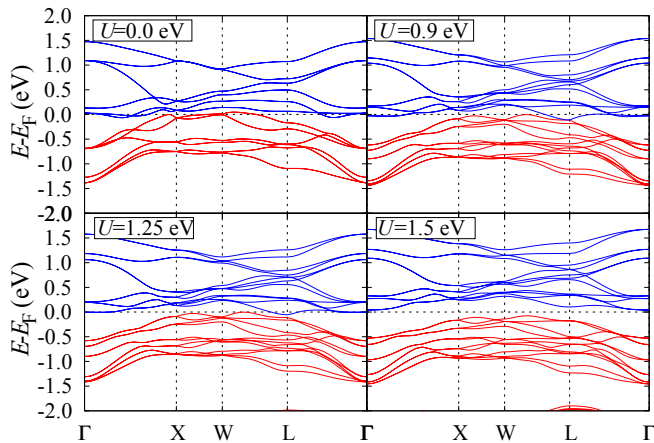


Figure 8. Band structure of $\text{Cd}_2\text{Os}_2\text{O}_7$ computed by the LDA+ U method. The result for $U = 0$ corresponds to the LDA band structure. For $U \geq 0.9$ eV, the ground states are all-in-all-out ordered states.

U_{eff} (eV)	J (meV)	A_{sia} (meV)	A_{DM} (meV)
1.25	14	24	4
2.0	35	41	0

Table 1. Nearest-neighbor exchange coupling, single-ion anisotropy and Dzyaloshinskii-Moriya (DM) interaction estimated by LDA+ U calculations for $\text{Cd}_2\text{Os}_2\text{O}_7$ and indicated values of $U_{\text{eff}} \equiv \bar{U} - \bar{J}$ [see Eq. (5)]. The direction vectors of the DM interaction are shown in Fig. 4(b) of Ref. [46].

6. Mott physics and magnetism in Ir pyrochlores

6.1. Phase diagram at half filling

The crossover between a paramagnetic metal and a paramagnetic insulator in Fig. 4 clearly indicates the importance of Mott physics in understanding the electronic properties of pyrochlore iridates. Mott physics in real compounds can be (partially) described by the LDA+DMFT method. As reviewed in section 7, the LDA+DMFT method can capture local correlation effects, including dynamical fluctuations. The LDA+DMFT method has been used to study various transition metal oxides (for a review, refer to Ref. [12]). However, the applicability of the method is still limited to a small class of compounds. When studying finite- T properties, the LDA+DMFT method is typically used in combination with continuous-time QMC calculations [61]. However, these CT-QMC calculations suffer from a sign problem at low temperature when multi-orbital aspects of the compound become relevant. In particular, the computation of magnetism in compounds with strong SOC still remains a challenging problem.

Figure 9 shows a theoretical phase diagram computed by DMFT calculations based on the LDA band structure of $\text{Y}_2\text{Ir}_2\text{O}_7$ (see Fig. 10) [55]. Some

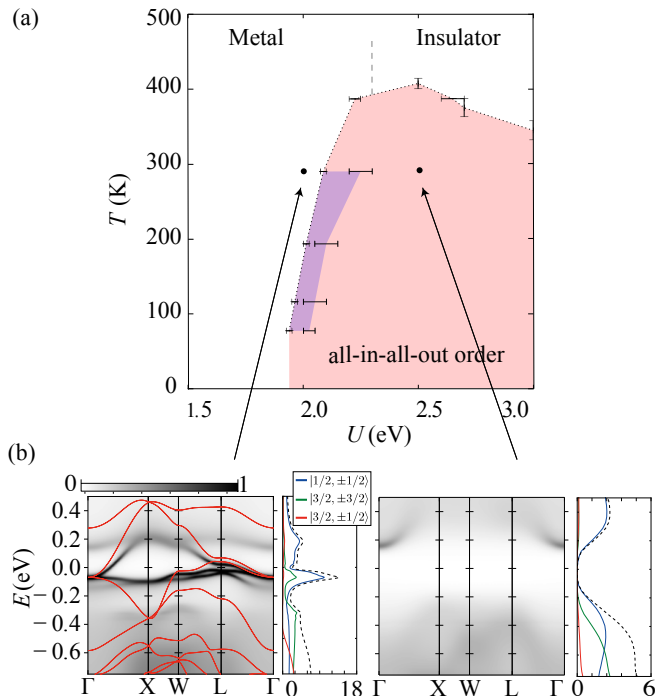


Figure 9. Phase diagram of $\text{Y}_2\text{Ir}_2\text{O}_7$ computed by LDA+DMFT [(a)]. The real compound may be located at $U \simeq 2.5$ eV. (b) Momentum-resolved spectral function computed at 290 K. The spectral functions projected onto the j_{eff} basis ($|j_{\text{eff}}, j_{\text{eff}}^{111}\rangle$) are also shown.

of us systematically explored the phase diagram by changing U (the Hund coupling parameter was fixed at $J_{\text{H}}/U = 1/10$). The large- U region in Fig. 9 corresponds to the small A -site ionic radius region in the experimental phase diagram (Fig. 4). There is a dome-shaped all-in-all-out magnetically ordered phase at large U , which extends up to about 400 K. It is empirically known that DMFT calculations for 3D compounds overestimate magnetic transition temperatures typically by a factor of 2–3 because of the neglect of spatial fluctuations. Considering this point, the experimental and theoretical phase diagram show a good agreement.

The broken line above the magnetic transition temperature indicates the crossover between a paramagnetic metal and a paramagnetic insulator. This can be identified by the gradual decrease of the spectral weight near the Fermi level as one moves from the small- U region to the large- U region. In the paramagnetic insulating region, the DC resistivity is expected to show an insulating behavior above the magnetic transition temperature. The target compound $\text{Y}_2\text{Ir}_2\text{O}_7$ exhibits insulating behavior of the resistivity at room temperature. Thus, $U \simeq 2.5$ eV may be a realistic value for the compound.

The lower panel of Fig. 9 shows the momentum-

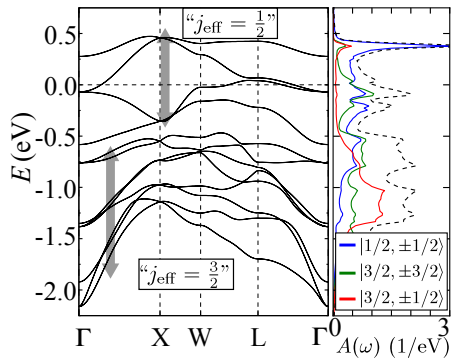


Figure 10. LDA band structure computed for $\text{Y}_2\text{Ir}_2\text{O}_7$. The density of states projected onto the j_{eff} basis is also shown.

resolved spectral function computed at 290 K.*. In the paramagnetic metallic region, quasi-particle bands of the $j_{\text{eff}}=1/2$ manifold are clearly observed. This $j_{\text{eff}}=1/2$ manifold shows a substantial band narrowing from the LDA value of $\simeq 1$ eV down to approximately 0.4 eV. In the insulating regime, the quasi-particle bands of the $j_{\text{eff}}=1/2$ manifold are smeared out, indicating its Mott nature.

Here comes an important question. How *relevant* is the role of the $j_{\text{eff}}=3/2$ manifold for $E < 0$? To answer this question, we first focus on the energy region ($E < -0.6$ eV) where the $j_{\text{eff}}=3/2$ bands are originally located before U is turned on. Even in the paramagnetic metallic region, these bands are smeared out and cannot be clearly identified. Another interesting observation is that the low-energy states consist mainly of the $j_{\text{eff}}=1/2$ orbitals for $\omega > 0$, while in LDA the $j_{\text{eff}}=3/2$ manifold contributes significantly to the density of states near $\omega = 0$ (see Fig. 10). A similar purification of the spectral function was found in the LDA+DMFT study of Sr_2IrO_4 [62].

These results indicate that the effects of the self-energy (refer to section 7) on the $j_{\text{eff}}=3/2$ manifold is substantial, which has nontrivial consequences. In LDA+DMFT calculations for the pyrochlore iridates, one can construct an effective one-band model for the $j_{\text{eff}}=1/2$ manifold, where the $j_{\text{eff}}=3/2$ manifold is neglected and is treated as frozen states. We confirmed that the dome-shaped all-in-all-out region is reduced in height by about a factor of two [63]. This indicates that the multi-orbital aspects may stabilize the all-in-all-out magnetic ordering, and thus, the three-orbital description is necessary for a quantitative understanding of this compound.

* To compute the spectral function, the (local) DMFT self-energy was continued to the real-frequency axis and then inserted into the Dyson equation, whose solution yields the lattice Green's function on the real-frequency axis.

As mentioned in Sec. 3.4, previous LDA+ U studies indicated the existence of a Weyl semimetallic phase between a magnetically ordered insulating phase and a paramagnetic metallic phase [49, 64]. The width of the Weyl semimetallic phase was estimated to be around 0.2 eV [64]. In contrast, in the LDA+DMFT phase diagram, no intermediate phase was found between the all-in-all-out magnetically ordered phase and the paramagnetic phase, which are separated by a first-order transition line at low T . This may indicate that the Weyl semimetallic phase is less stable under the influence of strong correlations (e.g., strong band-width renormalization). However, we must keep in mind that non-local correlations are neglected in single-site DMFT calculations, which may have a substantial effect near the magnetic quantum critical point. Therefore, the existence of such a non-trivial phase near the magnetic critical point still remains an open issue.

Recently, Prando *et al.* reported the magnetic properties of a related compound $\text{Eu}_2\text{Ir}_2\text{O}_7$ under hydrostatic pressure by macroscopic and local-probe techniques [65]. They found that the magnetic transition temperature increases up to $P = 20$ kbar and then drops as hydrostatic pressure is further increased. They compared their results with our theoretical results under the assumption that the hydrostatic pressure corresponds to changing the U/W ratio (W is the band width). Figure 11 shows a similar plot [66], where the theoretical transition temperature is scaled by a factor of 0.31 to correct the overestimation by the local approximation. One can see that the P dependence of the data is consistent with the theoretical curve, although experiments for higher P are needed for a more detailed comparison. While this comparison assumes that U/W changes as P is

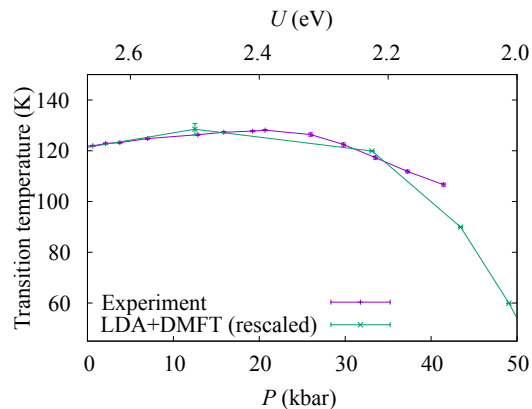


Figure 11. (Color online) Comparison of the pressure dependence of the critical transition temperature of $\text{Eu}_2\text{Ir}_2\text{O}_7$ and the LDA+DMFT results. The transition temperatures of LDA+DMFT were scaled by a factor of 0.31. We extracted the experimental data from Fig. 6 in Ref. [65].

increased, it remains to be clarified which microscopic parameters actually vary (see the related discussion in section 8).

6.2. Doped compounds

We next discuss the effects of carriers in pyrochlore iridates. An interesting observation in the spectral function computed by the DMFT method is the existence of nearly flat bands slightly above and below the Fermi level [see Fig. 9(b)]. These may get close to the Fermi level as the compound is doped with holes or electrons. Such effects were investigated by performing LDA+DMFT calculations with different numbers of electrons (without changing the non-interacting band structure) [55]. The LDA+DMFT calculations indicated the emergence of non-Fermi-liquid-like behavior down to low T (the lowest T computed was around 50 K) in the hole-doped cases. This can be understood in terms of long-lived local magnetic moments induced by the nearly flat bands down to low T .

Recently, hole-doped derivatives of $\text{Eu}_2\text{Ir}_2\text{O}_7$ were investigated through transport and magnetic measurements [67]. The metal-insulator transition temperature was found to get substantially reduced with hole doping, and for 10% Sr doping the composition is metallic down to temperatures as low as 5 K. This study found that these doped compositions violate the Mott-Ioffe-Regel condition for minimum electrical conductivity and show a distinct signature of non-Fermi liquid behavior at low temperature. The authors attributed this peculiar behavior to a disorder-induced variation of the spin-orbit-coupling parameter between Ir^{4+} and Ir^{5+} ions. However, the nearly flat bands may provide an alternative explanation.

7. Theoretical framework: LDA+ U and LDA+DMFT

In the previous sections, we have discussed rich phenomena arising from spin-orbital physics in $4d$ and $5d$ pyrochlores. The description of these phenomena such as non-collinear magnetism and Mott transitions requires the use of formalisms which go beyond the LDA. In this section, we provide a brief description of these methods for a comprehensive understanding of the technical advances underlying our studies. First, in section 7.1, we provide a brief description of the LDA+ U method, which was used to investigate the molybdates and osmate. In section 7.2, we explain the theory of maximally localized Wannier functions, on which all the studies shown in this review are based. In addition to these general theories, we also explain a convenient local coordinate system for pyrochlore oxides. These two sections furthermore

serve as an appetizer for the detailed discussion of the LDA+DMFT method in section 7.3. In section 7.3, we describe the basic theory of LDA+DMFT and some technical details especially on solving multi-orbital quantum impurity models. The solution of the DMFT impurity problem is one of the biggest bottlenecks in LDA+DMFT calculations for $4d$ and $5d$ systems due to a severe negative sign problem resulting from the SOC in Monte Carlo based techniques. We describe some recipe for avoiding a severe sign problem.

7.1. LDA+ U

Despite its success in the quantitative description of a wide range of materials, DFT with common approximations for the exchange-correlation functional, such as the local density approximation (LDA) and generalized gradient approximation (GGA), cannot properly capture electron-electron interaction effects in strongly correlated materials. A typical example is La_2CuO_4 , a mother compound of a copper-oxide superconductor. It is experimentally an antiferromagnetic insulator, whereas DFT-LDA yields a nonmagnetic metallic solution. Similar qualitatively wrong results are often obtained in transition-metal oxides. The error can be ascribed to the approximate exchange-correlation functional, and also to the local and static effective potential in the Kohn-Sham framework. This drawback is cured by explicitly introducing an on-site Coulomb repulsion (Hubbard U) [68, 69]. Let $\{n_{mm'}^\sigma\}$ be the density matrix of the interacting localized orbitals, e.g. the $3d$ orbitals. In the LDA+ U method, the total energy functional is written as

$$E^{\text{LDA}+U} = E^{\text{LSDA}} + E^U[\{n_{mm'}^\sigma\}] - E^{\text{dc}}[\{n_{mm'}^\sigma\}], \quad (1)$$

where E^{LSDA} is the total energy functional in the local spin-density approximation (LSDA), E^U represents the contribution from the Hubbard-type interaction, and E^{dc} is the double-counting term. Since the effects of E^U are partly included in E^{LSDA} , we have to remove the double counting by subtracting E^{dc} . There are several proposals for the explicit form of E^U and E^{dc} . One is a rotationally-invariant form by Liechtenstein *et al.* [70],

$$E^U = \frac{1}{2} \sum_{\{m\}, \sigma} \{ \langle m, m'' | V_{ee} | m', m''' \rangle n_{mm'}^\sigma n_{m''m'''}^{-\sigma} + (\langle m, m'' | V_{ee} | m', m''' \rangle - \langle m, m'' | V_{ee} | m''', m' \rangle) n_{mm'}^\sigma n_{m''m'''}^\sigma \}, \quad (2)$$

$$E^{\text{dc}} = \frac{1}{2} U n(n-1) - \frac{1}{2} J [n^\uparrow (n^\uparrow - 1) n^\downarrow (n^\downarrow - 1)], \quad (3)$$

where $n^\sigma = \text{Tr}(n_{mm'}^\sigma)$, $n = n^\uparrow + n^\downarrow$, and U and J are screened Coulomb and exchange interaction parameters, respectively. The corresponding effective one-electron potential becomes orbital-dependent:

$$\begin{aligned}
 V_{mm'}^\sigma &= \sum_{m'',m'''} \{ \langle m, m'' | V_{ee} | m', m''' \rangle n_{m''m'''}^{-\sigma} \\
 &\quad + (\langle m, m'' | V_{ee} | m', m''' \rangle \\
 &\quad - \langle m, m'' | V_{ee} | m''', m' \rangle) n_{m''m'''}^\sigma \} \\
 &\quad - U \left(n - \frac{1}{2} \right) + J \left(n^\sigma - \frac{1}{2} \right). \quad (4)
 \end{aligned}$$

Solovyev *et al.* [71] proposed a simpler form where the Coulomb interaction is spherically averaged. In our first-principles studies of the Os and Mo pyrochlores [35, 46], we used

$$\begin{aligned}
 E^{\text{LDA}+U} &= E^{\text{LSDA}} + \\
 &\quad \frac{\bar{U} - \bar{J}}{2} \sum_{\sigma} \left[\sum_m n_{mm}^\sigma - \sum_{mm'} n_{mm'}^\sigma n_{m'm}^\sigma \right], \quad (5)
 \end{aligned}$$

where \bar{U} and \bar{J} are spherically-averaged screened Coulomb and exchange interaction parameters, respectively [72].

Note that the relativistic effect including the SOC can be fully considered in solving the relativistic Kohn-Sham equation [73, 74]. The LDA+ U method can be regarded as a hybrid method in the sense that the DFT-LDA total energy is supplemented by the many-body terms associated with U and J in the Hartree-Fock approximation. The results depend on the choice of U and J . Although they are simply treated as adjustable parameters in many cases, there exist a few theoretical frameworks for evaluating them from first-principles, such as the constrained LDA [75, 76], linear-response approach [77], and constrained RPA method [78].

7.2. Construction of Wannier functions and local coordinate system

Localized orbitals need to be constructed for the formulation of low-energy effective tight-binding models and the implementation of methods like LDA+DMFT which are based on such effective tight-binding models. First-principles schemes based on localized orbitals as basis functions (LMTO and FLAPW *etc.*) directly provide the orbitals used in the LDA+DMFT calculations. A more general framework, which is applicable also to planewave methods, is the construction of Wannier functions. The Wannier function $\varphi_{n\mathbf{R}}(\mathbf{r})$ associated with a Bloch function $\psi_{n\mathbf{k}}(\mathbf{r})$ is defined as

$$\varphi_{n\mathbf{R}}(\mathbf{r}) = \frac{V}{(2\pi)^3} \int e^{-i\mathbf{k}\cdot\mathbf{R}} \psi_{n\mathbf{k}}(\mathbf{r}) d^3k, \quad (6)$$

where n is the orbital index, \mathbf{R} is the cell index, and \mathbf{k} is the wave vector. This Wannier function is not uniquely defined because the Bloch function has gauge degrees of freedom, $\psi_{n\mathbf{k}}(\mathbf{r}) \rightarrow e^{i\theta(\mathbf{k})} \psi_{n\mathbf{k}}(\mathbf{r})$. We may thus generalize the definition of the Wannier function as

$$\varphi_{n\mathbf{R}}(\mathbf{r}) = \frac{V}{(2\pi)^3} \int e^{-i\mathbf{k}\cdot\mathbf{R}} \tilde{\psi}_{n\mathbf{k}}(\mathbf{r}) d^3k, \quad (7)$$

$$\tilde{\psi}_{n\mathbf{k}}(\mathbf{r}) = \sum_m U_{mn}(\mathbf{k}) \psi_{m\mathbf{k}}(\mathbf{r}). \quad (8)$$

Namely, the Bloch functions are reconstructed by taking linear combinations of different bands. This is natural, because bands cross each other in \mathbf{k} -space, and hence there is no reason to limit n in Eq. (7) to a single band index throughout the whole Brillouin zone.

The maximally localized Wannier functions (MLWF) [79, 80, 81] utilize the gauge degrees of freedom, and determine the $U_{mn}(\mathbf{k})$ matrix such that the spread of the Wannier functions, defined by

$$\Omega = \sum_n [\langle \varphi_{n0} | r^2 | \varphi_{n0} \rangle - \langle \varphi_{n0} | r | \varphi_{n0} \rangle^2], \quad (9)$$

is minimized. Marzari and Vanderbilt have developed the formalism and a practical procedure to minimize the spread by the steepest descent method [79]. It was extended by Souza *et al.* to the case of entangled bands, where the Hilbert space spanned by the MLWF's is determined in such a way that $\tilde{\psi}_{n\mathbf{k}}(\mathbf{r})$ is as smooth as possible in \mathbf{k} -space [80].

The MLWF method has been applied to strongly-correlated systems in Refs. [82, 83, 84, 85]. In these studies, the MLWFs were used to define interacting localized orbitals, and U and J on the MLWFs are computed from first-principles in the constrained RPA [78].

In practical calculations, one provides an initial guess (initial orbitals) for the optimization of MLWFs. This may define the local coordinate system of the resulting tight-binding model. In our calculations for the Mo and Ir pyrochlores, for convenience, we used d_{xy} , d_{yz} , d_{zx} -like orbitals defined as initial orbitals in the local coordinate system with z aligned along [111], [-111], [1-11], or [11-1] on each of four Mo/Ir atoms [see Fig. 1(b)]. They are fully spin-polarized along the local z axis. The resulting tight-binding models are equivalent for each of the four atoms. To avoid any symmetry breaking in optimizing the Wannier functions, we projected the initial orbitals to the Bloch wave functions and did not further minimize the spread. Wannier functions constructed in this way are sometimes called ‘‘one-shot WF’s’’.

In the studies reviewed in this article, we took into account the effects of the SOC by constructing Wannier functions based on relativistic LDA calculations. In other words, the SOC appears in the tight-binding models in the form of single-particle terms.

7.3. LDA+DMFT

A more accurate treatment of local correlation effects is possible within the LDA+DMFT framework [11,

12], where the lattice system is mapped onto a self-consistently determined quantum impurity model. For this construction, we have to define localized (Wannier) orbitals for the t_{2g} states, and the corresponding local interaction

$$H_{\text{int}} = \frac{1}{2} \sum_{\alpha, \beta, \gamma, \delta, \sigma, \sigma'} U_{\alpha\beta\gamma\delta} d_{\alpha\sigma}^\dagger d_{\beta\sigma'}^\dagger d_{\gamma\sigma} d_{\delta\sigma}, \quad (10)$$

for which one typically considers the Slater-Kanamori form $U_{\alpha\alpha\alpha\alpha} = U$, $U_{\alpha\beta\alpha\beta} = U - 2J_{\text{H}}$, $U_{\alpha\beta\beta\alpha} = U_{\alpha\alpha\beta\beta} = J_{\text{H}}$ ($\alpha \neq \beta$). Here, α and σ are orbital and spin indices, while U and J_{H} denote the on-site repulsion and the Hund coupling, respectively. The self-consistency loop (Fig. 12) involves the calculation of the impurity Green's function G_{imp} and self-energy Σ for a given hybridization function Δ (or ‘‘Weiss’’ Green's function \mathcal{G}_0), the approximation of the lattice self-energy by the impurity self-energy (DMFT approximation), the calculation of the lattice Green's function for this approximate local self-energy, and finally the identification of the local lattice Green's function G_{loc} with the impurity Green's function G_{imp} (DMFT self-consistency condition). The last step allows to define the new hybridization function Δ (or \mathcal{G}_0) and this loop is iterated until convergence is reached. If the simulation is restricted to the t_{2g} subspace, and an orbital-independent double counting is adopted, it is sufficient to adjust the chemical potential to assure the proper filling. For more details on the DMFT self-consistent calculation, refer to Refs. [86, 12].

In the presence of SOC, one needs to treat complex and off-diagonal hybridization functions. As we will show later, one cannot diagonalize the hybridization functions by a basis transformation with respect to spin and orbital for pyrochlore oxides. The unbiased numerical solution of such multi-orbital impurity models has only become possible thanks to recent methodological developments.

7.3.1. Solution of the impurity problem We briefly discuss the hybridization expansion continuous-time Monte Carlo technique, which enables a numerically exact LDA+DMFT simulation of pyrochlore iridates down to a temperature of the order of 100 K.

Continuous-time impurity solvers [61] are based on an expansion of the partition function into a series of diagrams and the stochastic sampling of collections of these diagrams. The partition function of the impurity model is expressed as a sum (or, more precisely, integral) of the contributions w_C from all configurations C as

$$Z = \sum_C w_C, \quad (11)$$

where w_C can be complex. Note that the Hermitian property of the Hamiltonian ensures that Z is real after

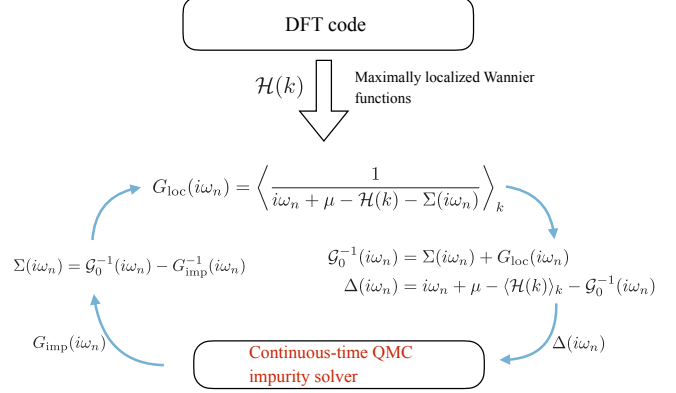


Figure 12. (Color online) Illustration of the DMFT self-consistency cycle. The most numerically expensive step is the solution of the impurity problem, i.e., the calculation of G_{imp} for a given Δ . $\langle \dots \rangle$ denotes an average over momentum space, and μ is the chemical potential.

the summation over C . This integral is evaluated by a random walk in configuration space $C_1 \rightarrow C_2 \rightarrow C_3 \rightarrow \dots$ with weight $|w_C|$. The random walk needs to be implemented in such a way that each configuration can be reached from any other in a finite number of steps (*ergodicity*) and that *detailed balance* is satisfied: $|w_{C_1}|p(C_1 \rightarrow C_2) = |w_{C_2}|p(C_2 \rightarrow C_1)$. This assures that each configuration C is generated with a probability proportional to $|w_C|$ and yields an estimate for some observable A based on a simple average over a finite number N of measurements:

$$\begin{aligned} \langle A \rangle &= \frac{\sum_C w_C A_C}{\sum_C w_C} = \frac{\sum_C |w_C| e^{i\varphi_C} A_C}{\sum_C |w_C| e^{i\varphi_C}} \\ &\approx \frac{\sum_{i=1}^N e^{i\varphi_{C_i}} A_{C_i}}{\sum_{i=1}^N e^{i\varphi_{C_i}}} = \frac{\langle e^{i\varphi} \cdot A \rangle_{\text{MC}}}{\langle e^{i\varphi} \rangle_{\text{MC}}}, \end{aligned} \quad (12)$$

where A_C is the value of the observable associated with the configuration C , $w_C = |w_C| e^{i\varphi_C}$ is split into the modulus and phase, and we assumed that A_C and w_C can be obtained by sampling the same configuration space. The error on this Monte Carlo estimate decreases like $1/\sqrt{N}$.

We focus here on general impurity models with Hamiltonian

$$H = H_{\text{loc}} + H_{\text{bath}} + H_{\text{hyb}}, \quad (13)$$

where H_{loc} describes the impurity, characterized by a small number of degrees of freedom (spin and orbital degrees of freedom denoted collectively by a, b, \dots), and H_{bath} describes an infinite reservoir of free electrons, labeled by a continuum of quantum numbers p and a discrete set of quantum numbers α . Finally, H_{hyb} describes the exchange of electrons between

the impurity and the bath in terms of hybridization amplitudes $V_p^{a\alpha}$. Explicitly, the three terms are

$$H_{\text{loc}} = \sum_{ab} \epsilon^{ab} d_a^\dagger d_b + \frac{1}{2} \sum_{abcd} U^{abcd} d_a^\dagger d_b^\dagger d_c d_d, \quad (14)$$

$$H_{\text{bath}} = \sum_{p\alpha} \epsilon_{p\alpha} c_{p\alpha}^\dagger c_{p\alpha}, \quad (15)$$

$$H_{\text{hyb}} = \sum_{p\alpha} [V_p^{a\alpha} d_a^\dagger c_{p\alpha} + (V_p^{a\alpha})^* c_{p\alpha}^\dagger d_a]. \quad (16)$$

The hybridization-expansion approach [87, 88] is based on an expansion of the partition function Z in powers of the impurity-bath hybridization term, H_{hyb} , and an interaction representation in which the time evolution is determined by $H_{\text{loc}} + H_{\text{bath}}$: $O(\tau) = e^{\tau(H_{\text{loc}}+H_{\text{bath}})} O e^{-\tau(H_{\text{loc}}+H_{\text{bath}})}$.

Since $H_{\text{hyb}} \equiv H_{\text{hyb}}^{d^\dagger} + H_{\text{hyb}}^d = \sum_{p\alpha} V_p^{a\alpha} d_a^\dagger c_{p\alpha} + \sum_{p\alpha} (V_p^{a\alpha})^* c_{p\alpha}^\dagger d_a$ has two terms, corresponding to electrons hopping from the bath to the impurity and from the impurity back to the bath, only even perturbation orders appear in the expansion of Z . Furthermore, at perturbation order $2n$, only the $(2n)!/(n!)^2$ terms corresponding to n creation operators d^\dagger and n annihilation operators d contribute. We therefore write the partition function as a sum over configurations $\{\tau_1, \dots, \tau_n; \tau'_1, \dots, \tau'_n\}$ that are collections of imaginary-time points corresponding to these n annihilation and n creation operators:

$$Z = \sum_{n=0}^{\infty} \int_0^\beta d\tau_1 \cdots \int_{\tau_{n-1}}^\beta d\tau_n \int_0^\beta d\tau'_1 \cdots \int_{\tau'_{n-1}}^\beta d\tau'_n \\ \times \text{Tr} \left[e^{-\beta H_1} \mathcal{T} H_{\text{hyb}}^d(\tau_n) H_{\text{hyb}}^{d^\dagger}(\tau'_n) \cdots H_{\text{hyb}}^d(\tau_1) H_{\text{hyb}}^{d^\dagger}(\tau'_1) \right].$$

Introducing the β -antiperiodic hybridization function Δ , which in the Matsubara-frequency representation reads

$$\Delta_{ab}(i\omega_n) = \sum_{p,\alpha} \frac{(V_p^{a\alpha})^* (V_p^{b\alpha})}{i\omega_n - \epsilon_{p\alpha}},$$

we can explicitly evaluate the trace over the bath states to find $Z_{\text{bath}} \det M^{-1}$, where M^{-1} is an $(n \times n)$ matrix with elements

$$[M^{-1}]_{ij} = \Delta_{a'_i a_j}(\tau_i^{a'_i} - \tau_j^{a_j}). \quad (17)$$

In the hybridization expansion approach, the configuration space thus consists of all sequences $C = \{\tau_1^{a_1}, \dots, \tau_n^{a_n}; \tau'_1{}^{a'_1}, \dots, \tau'_n{}^{a'_n}\}$ of n creation and n annihilation operators ($n = 0, 1, \dots$), and the weight of such a configuration is

$$w_C = Z_{\text{bath}} \text{Tr} \left[e^{-\beta H_{\text{loc}}} \mathcal{T} d_{a_n}(\tau_n^{a_n}) d_{a'_n}^\dagger(\tau'_n{}^{a'_n}) \cdots \right. \\ \left. \cdots d_{a_1}(\tau_1^{a_1}) d_{a'_1}^\dagger(\tau'_1{}^{a'_1}) \right] \det M^{-1} (d\tau)^{2n}.$$

The trace factor represents the contribution of the impurity, which fluctuates between different quantum states as electrons hop in and out, while the

determinant sums up all bath evolutions which are compatible with the given sequence of transitions.

The hybridization functions can in general be off-diagonal ($\Delta_{ab} \neq 0$ for $a \neq b$) and complex and the trace factor also can be complex in the presence of SOC. This typically leads to complex configuration weights w_C , and to a sign problem (or more properly phase problem) in the Monte Carlo sampling. We can implement a Monte Carlo sampling using the positive distribution of weights $|w_C|$, and shift the phase to the observable. As shown in Eq. (12), the expectation values of observables are then obtained by the ratio of the phase weighted measurement and the average value of the phase. Note that while $w_C/|w_C|$ can be a complex number, the expectation value $\langle e^{i\varphi} \rangle$, which is usually denoted by ‘‘average sign’’, is always real because the partition function is real.

An open source hybridization expansion continuous-time Monte Carlo impurity solver, which handles off-diagonal and complex hybridizations, and thus is suitable for the LDA+DMFT study of pyrochlore iridates, has recently been published in Ref. [89].

7.3.2. Sign problem and choice of local basis The sign problem strongly depends on the local basis in which the hybridization expansion is performed. By transforming from orbitals $\{\alpha\}$ to new orbitals $\{\alpha'\}$ we change the hybridization functions, and hence the diagrams which are sampled. Typically, the sign problem is severe if the off-diagonal components of the hybridization function are large.

In some previous studies of pyrochlore iridates, the quantum impurity models for $5d$ electrons have been simplified to avoid a severe sign problem by omitting off-diagonal hybridization functions and some interaction terms in the j_{eff} basis. However, since pyrochlore iridates have large inter-band hybridizations, one should avoid such approximations. The exact treatment also does not assume the quantization axes of spin and orbital. The sign problem in calculations with full hybridization matrix can to some extent be reduced by rotating the single-particle basis of the hybridization function.

Specifically, for the calculations in Fig. 9, we solved the quantum impurity problem by Monte Carlo sampling in a basis which diagonalizes the local SOC in the t_{2g} manifold. This eigenbasis was constructed by numerically diagonalizing the non-interacting Hamiltonian on an Ir atom. Although the basis vectors correspond to the three doublets shown in the diagram of Fig. 2(b), the phase degrees of freedom in each doublet were numerically fixed. Thus, the basis functions are eigenvectors of $(\hat{j}_{\text{eff}}^{111})^2$ but not $\hat{j}_{\text{eff}}^{111}$.[‡] In the eigenbasis, we observed substantial off-

[‡] We did not observe any significant dependence of the average

site hybridization functions between the lowest and the highest doublets, leading to a sign problem in the Monte Carlo sampling. We took into account all the off-diagonal hybridization functions using the impurity solver of Ref. [89].

Figure 13 shows the average sign encountered in solving the quantum impurity problems. The calculations were done for $J_H = 0.1U$ down to $\beta = 150$ (1/eV), corresponding to 77 K. The average sign remains sufficiently large in the eigenbasis that calculations can be performed with modest computational resources. Interestingly, the temperature dependence of the sign is not monotonic. At large U , the average sign shows a local minimum around 200 K, recovers, and then decreases again below 100 K. Although this basis may not be optimal in terms of average sign, it turns out to be good enough for the purpose of mapping out the phase diagram of $Y_2Ir_2O_7$.

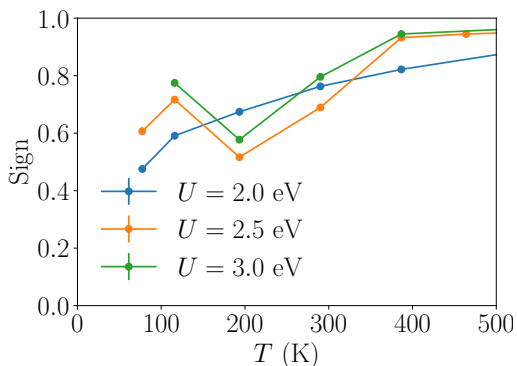


Figure 13. (Color online) Average sign encountered in solving the DMFT quantum impurity problem for pyrochlore iridates. The average sign remains above 0.4 down to 77 K for $U = 2.5$ and 3 eV.

8. Summary and future perspectives

In this article, we have reviewed our first-principles studies on $4d$ and $5d$ pyrochlore oxides, where spin-orbital physics plays a substantial role. We showed that in the insulating Mo pyrochlores, the interplay of spin and orbital under the SOC is relevant to the magnetic properties such as the puzzling spin-glass behavior. The SOC also plays an important role in stabilizing the non-collinear magnetic order and determining the metal-insulator transition in the Os compound $Cd_2Os_2O_7$. For the Ir pyrochlores, LDA+DMFT calculations within a three-orbital description qualitatively reproduce the experimental phase diagram, and we emphasized the importance of the multi-orbital nature. We also

sign on the choice of the phase degrees of freedom within the doublets.

reviewed the theoretical frameworks used in these studies.

Let us briefly discuss the future direction of first-principles studies on pyrochlore oxides and related compounds. In section 6.1, the on-site U was considered to be a control parameter for the metal-insulator transition at half filling in pyrochlore iridates. However, is this *assumption* really correct? Which microscopic parameters change as we go through the metal-insulator transition in Fig. 4? This is an open issue which touches on fundamental properties of the pyrochlore iridates. In the supplemental material of Ref. [20], using the LDA+DMFT calculations, Zhang *et al.* pointed out the important role of the internal oxygen coordinate x in determining the ground state of the pyrochlore iridates. On the other hand, a recent cluster DMFT study of single-orbital tight-binding models indicated the importance of intersite magnetic correlations in the qualitative description of the A -site dependence [90]. These effects are not captured by single-site(atom) LDA+DMFT calculations. Thus, a comprehensive understanding of the metal-insulator transition is still missing.

Another interesting topic for $5d$ pyrochlores is the design of non-trivial quantum phases at surfaces, magnetic domain boundaries, or in superlattice structures. Recently, the existence of metallic states at magnetic domain boundaries has been confirmed experimentally for $Cd_2Os_2O_7$ [91], $Eu_2Ir_2O_7$ [92, 93], and $Nd_2Ir_2O_7$ [94]. On the other hand, it has been theoretically shown that such magnetic boundaries can host metallic states with non-trivial topological properties [95, 96]. Furthermore, there are interesting theoretical proposals for topological phenomena in thin films of pyrochlore iridates [97, 98]. Designing such non-trivial quantum phases by first-principles calculations may be an interesting topic.

Recently, the $5d$ pyrochlore $Cd_2Re_2O_7$ with a $5d^2$ configuration has attracted much attention. This compound is unique in the sense that among the (α -)pyrochlores, it is the only one which shows superconductivity (at $T \simeq 1$ K) [99, 100, 101], and hosts various unidentified (likely) electronic phases. At ambient pressure, the compound exhibits two successive structural transitions at $T \simeq 200$ K and $T \simeq 120$ K [101, 102, 103, 104, 105, 106, 107, 108, 109, 110]. Despite drastic changes in the electronic properties below these transition temperatures [111, 112], only tiny structural changes were observed, indicating that their origins are electronic. A recent experimental study has reported the emergence of multipolar phases below these transition temperatures [108]. It was also suggested that this compound is a prototype of the spin-orbit-coupled metal recently proposed in Ref. [113]. The nature of these transitions is however

under debate. Remarkably, at high pressures, the compound exhibits an even richer structural phase diagram [114].

There obviously remains a broad spectrum of interesting and unsolved problems, especially in the study of 5d pyrochlores. Theoretical investigations of these compounds will play an important role in clarifying the relevant physical processes, and these applications will mark a frontier of modern first-principles simulations of correlated systems.

Acknowledgments

HS and PW acknowledge support from the DFG via FOR 1346, from SNF Grant No. 200021E-149122, ERC Advanced Grant SIMCOFE and NCCR MARVEL.

- [1] Masatoshi Imada, Atsushi Fujimori, and Yoshinori Tokura. Metal-insulator transitions. *Reviews of Modern Physics*, 70(4):1039–1263, 1998.
- [2] Michael R. Norman. The challenge of unconventional superconductivity. *Science*, 332(6026):196–200, 2011.
- [3] G. R. Stewart. Unconventional superconductivity. *Advances in Physics*, 66(2):75–196, 2017.
- [4] Manfred Fiebig. Revival of the magnetoelectric effect. *Journal of Physics D: Applied Physics*, 38(8):R123, 2005.
- [5] Manfred Fiebig, Thomas Lottermoser, Dennis Meier, and Morgan Trassin. The evolution of multiferroics. *Nature Reviews Materials*, 1:16046, 2016.
- [6] M A Subramanian, G Aravamudan, and GVS Rao. Oxide Pyrochlores - a Review. *Progress in Solid State Chemistry*, 15(2):55–143, 1983.
- [7] Jason S Gardner, Michel J P Gingras, and John E Greedan. Magnetic pyrochlore oxides. *Reviews of Modern Physics*, 82(1):53–107, January 2010.
- [8] P Hohenberg and W Kohn. Inhomogeneous Electron Gas. *Phys.Rev.*, 136(3B):B864–B871, 1964.
- [9] Walter Kohn and Lu Jeu Sham. Self-consistent equations including exchange and correlation effects. *Physical Review*, 140(4A):A1133, 1965.
- [10] Masatoshi Imada and Takashi Miyake. Electronic Structure Calculation by First Principles for Strongly Correlated Electron Systems. *Journal of the Physical Society of Japan*, 79(11):112001–42, November 2010.
- [11] K Held, I A Nekrasov, N Blümer, VI Anisimov Journal of Modern, and 2001. Realistic modeling of strongly correlated electron systems: An introduction to the LDA+ DMFT approach. *International Journal of Modern Physics B*, 15(19n20):2611–2625, August 2001.
- [12] G Kotliar, S Y Savrasov, K Haule, V Oudovenko, O Parcollet, and C Marianetti. Electronic structure calculations with dynamical mean-field theory. *Reviews of Modern Physics*, 78(3):865–951, August 2006.
- [13] Y P Huang, G Chen, and Michael Hermele. Quantum spin ices and topological phases from dipolar-octupolar doublets on the pyrochlore lattice. *Physical Review Letters*, 112:167203, April 2014.
- [14] Gang Chen and Michael Hermele. Magnetic orders and topological phases from f-d exchange in pyrochlore iridates. *Physical Review B*, 86(23):235129–7, December 2012.
- [15] Xu-Ping Yao and Gang Chen. Pr2Ir2O7: When Luttinger Semimetal Meets Melko-Hertog-Gingras Spin Ice State. *Physical Review X*, 8(4):041039, December 2018.
- [16] B Kim, Hosub Jin, S Moon, J Y Kim, B G Park, C Leem, Jaemun Yu, T Noh, C Kim, S J Oh, J H Park, V Durairaj, G Cao, and E Rotenberg. Novel Jeff=1/2 Mott State Induced by Relativistic Spin-Orbit Coupling in Sr2IrO4. *Physical Review Letters*, 101(7):076402, August 2008.
- [17] B J Kim, H Ohsumi, T Komesu, S Sakai, T Morita, H Takagi, and T Arima. Phase-Sensitive Observation of a Spin-Orbital Mott State in Sr2IrO4. *Science*, 323(5):1329, March 2009.
- [18] Satoru Sugano. *Multiplets of Transition-Metal Ions in Crystals*. Academic Press, 1970.
- [19] L Hozoi, H Gretarsson, J P Clancy, B G Jeon, B Lee, K H Kim, V Yushankhai, Peter Fulde, D Casa, T Gog, Jung-ho Kim, A H Said, M H Upton, Young-June Kim, and Jeroen van den Brink. Longer-range lattice anisotropy strongly competing with spin-orbit interactions in pyrochlore iridates. *Physical Review B*, 89(11):115111, March 2014.
- [20] Hongbin Zhang, Kristjan Haule, and David Vanderbilt. Metal-Insulator Transition and Topological Properties of Pyrochlore Iridates. *Physical Review Letters*, 118(2):026404, January 2017.
- [21] Mineo Sato, Xu Yan, and J E Greedan. Magnetic properties and magnetic ordering in the Rare Earth Molybdenum(IV) Pyrochlores: R2Mo2O7. *Zeitschrift für anorganische und allgemeine Chemie*, 540(9-10):177–190, September 1986.
- [22] T Katsufuji, H Y Hwang, and S W Cheong. Anomalous Magnetotransport Properties of R2Mo2O7 near the Magnetic Phase Boundary. *Physical Review Letters*, 84(9):1998–2001, February 2000.
- [23] M J P Gingras, C V Stager, N P Raju, B D Gaulin, and J E Greedan. Static Critical Behavior of the Spin-Freezing Transition in the Geometrically Frustrated Pyrochlore Antiferromagnet Y2Mo2O7. *Physical Review Letters*, 78(5):947–950, 1997.
- [24] G Prando, P Carretta, A U B Wolter, R Saint-Martin, A Revcolevschi, and B Büchner. Amorphous ferromagnetism and re-entrant magnetic glassiness in single-crystalline Sm2Mo2O7. *Physical Review B*, 90(8):085111–14, August 2014.
- [25] I V Solovyev. Effects of crystal structure and on-site Coulomb interactions on the electronic and magnetic structure of A2Mo2O7 (A=Y, Gd, and Nd) pyrochlores. *Physical Review B*, 67(17):174406, May 2003.
- [26] K Binder and A P Young. Spin glasses: Experimental facts, theoretical concepts, and open questions. *Reviews of Modern Physics*, 58(4):801–976, 1986.
- [27] C H Booth, J S Gardner, G H Kwei, R H Heffner, F Bridges, and M A Subramanian. Local lattice disorder in the geometrically-frustrated spin glass pyrochlore Y2Mo2O7. *Physical Review B*, 62(2):R755–R758, July 2000.
- [28] S Iguchi, N Hanasaki, M Kinuhara, N Takeshita, C Terakura, Y Taguchi, H Takagi, and Y Tokura. Emergence of a Diffusive Metal State with No Magnetic Order near the Mott Transition in Frustrated Pyrochlore-Type Molybdates. *Physical Review Letters*, 102(13):136407–4, April 2009.
- [29] N Hanasaki, K Watanabe, T Ohtsuka, I Kézsmárki, S Iguchi, S Miyasaka, and Y Tokura. Nature of the Transition between a Ferromagnetic Metal and a Spin-Glass Insulator in Pyrochlore Molybdates. *Physical Review Letters*, 99(8):086401–4, August 2007.
- [30] T Saunders and J Chalker. Spin Freezing in Geometrically Frustrated Antiferromagnets with Weak Disorder. *Physical Review Letters*, 98(15):157201, April 2007.
- [31] A Andreanov, J T Chalker, T E Saunders, and D Sherrington. Spin-glass transition in geometrically frustrated

- antiferromagnets with weak disorder. *Physical Review B*, 81(1):014406, January 2010.
- [32] Hiroshi Shinaoka, Yusuke Tomita, and Yukitoshi Motome. Spin-Glass Transition in Bond-Disordered Heisenberg Antiferromagnets Coupled with Local Lattice Distortions on a Pyrochlore Lattice. *Physical Review Letters*, 107(4):047204, July 2011.
- [33] Hiroshi Shinaoka, Yusuke Tomita, and Yukitoshi Motome. Effect of magnetoelastic coupling on spin-glass behavior in Heisenberg pyrochlore antiferromagnets with bond disorder. *Physical Review B*, 90(16):165119, October 2014.
- [34] H J Silverstein, K Fritsch, F Flicker, A M Hallas, J S Gardner, Y Qiu, G Ehlers, A T Savici, Z Yamani, K A Ross, B D Gaulin, M J P Gingras, J A M Paddison, K Foyevtsova, R Valenti, F Hawthorne, C R Wiebe, and H D Zhou. Liquidlike correlations in single-crystalline Y₂Mo₂O₇: An unconventional spin glass. *Physical Review B*, 89(5):054433, February 2014.
- [35] Hiroshi Shinaoka, Yukitoshi Motome, Takashi Miyake, and Shoji Ishibashi. Spin-orbital frustration in molybdenum pyrochlores A₂Mo₂O₇ (A= rare earth). *Physical Review B*, 88(17):174422, November 2013.
- [36] Kazuyuki Matsuhira, Makoto Wakeshima, Yukio Hinatsu, and Seishi Takagi. Metal-Insulator Transitions in Pyrochlore Oxides Ln₂Ir₂O₇. *Journal of the Physical Society of Japan*, 80(9):094701, September 2011.
- [37] K Ueda, J Fujioka, and Y Tokura. Variation of optical conductivity spectra in the course of bandwidth-controlled metal-insulator transitions in pyrochlore iridates. *Physical Review B*, 93(24):245120, June 2016.
- [38] A W Sleight, J L Gillson, J F Weiher, and W Bindloss. Semiconductor-metal transition in novel Cd₂O_s2O₇. *Solid State Communications*, 14(4):357-359, February 1974.
- [39] D Mandrus, J Thompson, R Gaal, L Forro, J Bryan, B Chakoumakos, L Woods, B Sales, R Fishman, and V Keppens. Continuous metal-insulator transition in the pyrochlore Cd₂O_s2O₇. *Physical Review B*, 63(19):195104, April 2001.
- [40] W J Padilla, D Mandrus, and D N Basov. Searching for the Slater transition in the pyrochlore Cd₂O_s2O₇ with infrared spectroscopy. *Physical Review B*, 66(3):035120, July 2002.
- [41] H Harima. Electronic bandstructures on 5d-transition metal pyrochlore: Cd₂Re₂O₇ and Cd₂Os₂O₇. *Journal of Physics and Chemistry of Solids*, 63(6-8):1035-1038, 2002.
- [42] D J Singh, P Blaha, K Schwarz, and J O Sofo. Electronic structure of the pyrochlore metals Cd₂O_s2O₇ and Cd₂Re₂O₇. *Physical Review B*, 65(15):155109, March 2002.
- [43] Akihiro Koda, Ryosuke Kadono, Kazuki Ohishi, Shanta R Saha, Wataru Higemoto, Shigeki Yonezawa, Yuji Muraoka, and Zenji Hiroi. Anomalous Magnetic Phase in an Undistorted Pyrochlore Oxide Cd₂O_s2O₇ Induced by Geometrical Frustration. *Journal of the Physical Society of Japan*, 76(6):063703, June 2007.
- [44] Y H Matsuda, J L Her, S Michimura, T Inami, M Suzuki, N Kawamura, M Mizumaki, K Kindo, J Yamamura, and Z Hiroi. Orbital magnetism in Cd₂O_s2O₇ studied by x-ray magnetic circular dichroism. *Physical Review B*, 84(17):174431, November 2011.
- [45] J Yamamura, K Ohgushi, H Ohsumi, T Hasegawa, I Yamauchi, K Sugimoto, S Takeshita, A Tokuda, M Takata, M Udagawa, M Takigawa, H Harima, T Arima, and Z Hiroi. Tetrahedral Magnetic Order and the Metal-Insulator Transition in the Pyrochlore Lattice of Cd₂O_s2O₇. *Physical Review Letters*, 108(24):247205, June 2012.
- [46] Hiroshi Shinaoka, Takashi Miyake, and Shoji Ishibashi. Noncollinear Magnetism and Spin-Orbit Coupling in 5d Pyrochlore Oxide Cd₂O_s2O₇. *Physical Review Letters*, 108(24):247204, June 2012.
- [47] D Yanagishima, Daiki Yanagishima, and Yoshiteru Maeno. Metal-Nonmetal Changeover in Pyrochlore Iridates. *Journal of the Physical Society of Japan*, 70(10):2880-2883, October 2001.
- [48] N Taira, M Wakeshima, and Y Hinatsu. Magnetic properties of iridium pyrochlores R₂Ir₂O₇ (R= Y, Sm, Eu and Lu). *Journal of Physics: Condensed matter*, 13(23):5527-5533, 2001.
- [49] Xiangang Wan, Ari M Turner, Ashvin Vishwanath, and Sergey Y Savrasov. Topological semimetal and Fermi-arc surface states in the electronic structure of pyrochlore iridates. *Physical Review B*, 83(20):205101, May 2011.
- [50] Keisuke Tomiyasu, Kazuyuki Matsuhira, Kazuaki Iwasa, Masanori Watahiki, Seishi Takagi, Makoto Wakeshima, Yukio Hinatsu, Makoto Yokoyama, Kenji Ohoyama, and Kazuyoshi Yamada. Emergence of Magnetic Long-range Order in Frustrated Pyrochlore Nd₂Ir₂O₇ with Metal-Insulator Transition. *Journal of the Physical Society of Japan*, 81(3):034709, March 2012.
- [51] H Sagayama, D Uematsu, T Arima, K Sugimoto, J J Ishikawa, E O'Farrell, and S Nakatsuji. Determination of long-range all-in-all-out ordering of Ir 4+ moments in a pyrochlore iridate Eu₂Ir₂O₇ by resonant x-ray diffraction. *Physical Review B*, 87(10):100403(R), March 2013.
- [52] Retno Asih, Noraina Adam, Saidah Sakinah Mohd-Tajudin, Dita Puspita Sari, Kazuyuki Matsuhira, Hanjie Guo, Makoto Wakeshima, Yukio Hinatsu, Takehito Nakano, Yasuo Nozue, Shukri Sulaiman, Mohamad Ismail Mohamed-Ibrahim, Pabitra Kumar Biswas, and Isao Watanabe. Magnetic Moments and Ordered States in Pyrochlore Iridates Nd₂Ir₂O₇ and Sm₂Ir₂O₇ Studied by Muon-Spin Relaxation. *Journal of the Physical Society of Japan*, 86(2):024705, February 2017.
- [53] Takeshi Kondo, M Nakayama, R Chen, J J Ishikawa, E G Moon, T Yamamoto, Y Ota, W Malaeb, H Kanai, Y Nakashima, Y Ishida, R Yoshida, H Yamamoto, M Matsunami, S Kimura, N Inami, K Ono, H Kumigashira, S Nakatsuji, L Balents, and S Shin. Quadratic Fermi node in a 3D strongly correlated semimetal. *Nature Communications*, 6(1):10042, November 2015.
- [54] A B Sushkov, J B Hofmann, G S Jenkins, J Ishikawa, S Nakatsuji, S Das Sarma, and H D Drew. Optical evidence for a Weyl semimetal state in pyrochlore Eu₂Ir₂O₇. *Physical Review B*, 92(24):241108(R), December 2015.
- [55] Hiroshi Shinaoka, Shintaro Hoshino, Matthias Troyer, and Philipp Werner. Phase Diagram of Pyrochlore Iridates: All-in-All-out Magnetic Ordering and Non-Fermi-Liquid Properties. *Physical Review Letters*, 115(15):156401-5, October 2015.
- [56] Peter M M Thygesen, Joseph A M Paddison, Ronghuan Zhang, Kevin A Beyer, Karena W Chapman, Helen Y Playford, Matthew G Tucker, David A Keen, Michael A Hayward, and Andrew L Goodwin. Orbital Dimer Model for the Spin-Glass State in Y₂Mo₂O₇. *Physical Review Letters*, 118(6), 2017.
- [57] C H Sohn, Hgyun Jeong, Hosub Jin, Soyeon Kim, L J Sandilands, H J Park, K W Kim, S J Moon, Deok-Yong Cho, J Yamamura, Z Hiroi, and T W Noh. Optical Spectroscopic Studies of the Metal-Insulator Transition Driven by All-In-All-Out Magnetic Ordering in 5d Pyrochlore Cd₂O_s2O₇. *Physical Review Letters*, 115(26):266402, December 2015.

- [58] Z Hiroi, J Yamaura, T Hirose, I Nagashima, and Y Okamoto. Lifshitz metal-insulator transition induced by the all-in/all-out magnetic order in the pyrochlore oxide $\text{Cd}_2\text{Os}_2\text{O}_7$. *APL Materials*, 3(4):041501, April 2015.
- [59] J G Vale, N A Bogdanov, X Liu, C Donnerer, M H Upton, D Casa, A H Said, M D Lumsden, Z Zhao, J Q Yan, D Mandrus, S Nishimoto, J Van Den Brink, J P Hill, D F McMorro, A D Christianson, and S Calder. Spin-orbit-driven magnetic structure and excitation in the 5d pyrochlore $\text{Cd}_2\text{Os}_2\text{O}_7$. *Nature Communications*, 7:1–8, May 2016.
- [60] Thi Minh Hien Nguyen, Luke J Sandilands, C H Sohn, C H Kim, Aleksander L Wysocki, In-Sang Yang, S J Moon, Jae-Hyeon Ko, J Yamaura, Z Hiroi, and Tae Won Noh. Two-magnon scattering in the 5d all-in-all-out pyrochlore magnet $\text{Cd}_2\text{Os}_2\text{O}_7$. *Nature Communications*, 2017(Aug):1–7, October 2017.
- [61] Emanuel Gull, Andrew J Millis, Alexander I Lichtenstein, Alexey N Rubtsov, Matthias Troyer, and Philipp Werner. Continuous-time Monte Carlo methods for quantum impurity models. *Reviews of Modern Physics*, 83(2):349–404, May 2011.
- [62] Hongbin Zhang, Kristjan Haule, and David Vanderbilt. Effective $J=1/2$ Insulating State in Ruddlesden-Popper Iridates: An LDA+DMFT Study. *Physical Review Letters*, 111(24):246402, December 2013.
- [63] H. Shinaoka, S. Hoshino, M. Troyer, P. Werner, unpublished.
- [64] Fumiyuki Ishii, Yo Pierre Mizuta, Takehiro Kato, Taisuke Ozaki, Hongming Weng, and Shigeki Onoda. First-Principles Study on Cubic Pyrochlore Iridates $\text{Y}_2\text{Ir}_2\text{O}_7$ and $\text{Pr}_2\text{Ir}_2\text{O}_7$. *Journal of the Physical Society of Japan*, 84(7):073703, July 2015.
- [65] G Prando, R Dally, W Schottenhamel, Z Guguchia, S H Baek, R Aeschlimann, A U B Wolter, S D Wilson, B Büchner, and M J Graf. Influence of hydrostatic pressure on the bulk magnetic properties of $\text{Eu}_2\text{Ir}_2\text{O}_7$. *Physical Review B*, 93(10):104422, March 2016.
- [66] H Shinaoka, F Assaad, N Blümer, and P Werner. Quantum Monte Carlo impurity solvers for multi-orbital problems and frequency-dependent interactions. *The European Physical Journal Special Topics*, 226(11):2499–2523, July 2017.
- [67] A Banerjee, J Sannigrahi, S Giri, and S Majumdar. Observation of non-Fermi liquid behavior in hole-doped $\text{Eu}_2\text{Ir}_2\text{O}_7$. *Physical Review B*, 96(22):224426, December 2017.
- [68] Vladimir I Anisimov, Jan Zaanen, and Ole K Andersen. Band theory and mott insulators: Hubbard u instead of stoner i . *Physical Review B*, 44(3):943, 1991.
- [69] Vladimir I Anisimov, Ferdi Aryasetiawan, and AI Lichtenstein. First-principles calculations of the electronic structure and spectra of strongly correlated systems: the $\text{Lda}+u$ method. *Journal of Physics: Condensed Matter*, 9(4):767, 1997.
- [70] AI Lichtenstein, VI Anisimov, and J Zaanen. Density-functional theory and strong interactions: Orbital ordering in mott-hubbard insulators. *Physical Review B*, 52(8):R5467, 1995.
- [71] I V Solovyev, P H Dederichs, and V I Anisimov. Corrected Atomic Limit in the Local-Density Approximation and the Electronic-Structure of D-Impurities in Rb. *Physical Review B*, 50(23):16861–16871, 1994.
- [72] SL Dudarev, GA Botton, SY Savrasov, CJ Humphreys, and AP Sutton. Electron-energy-loss spectra and the structural stability of nickel oxide: An $\text{LSDA}+u$ study. *Physical Review B*, 57(3):1505, 1998.
- [73] Tatsuki Oda, Alfredo Pasquarello, and Roberto Car. Fully Unconstrained Approach to Noncollinear Magnetism: Application to Small Fe Clusters. *Physical Review Letters*, 80(1):3622–3625, April 1998.
- [74] Taichi Kosugi, Takashi Miyake, and Shoji Ishibashi. Slab Thickness Dependence of Rashba Splitting on $\text{Au}(111)$ Surface: First-Principles and Model Analyses. *Journal of the Physical Society of Japan*, 80(7):074713, July 2011.
- [75] O Gunnarsson, OK Andersen, O Jepsen, and J Zaanen. Density-functional calculation of the parameters in the anderson model: Application to mn in cdte . *Physical Review B*, 39(3):1708, 1989.
- [76] O Gunnarsson. Calculation of parameters in model hamiltonians. *Phys. Rev. B*, 41:514, 1990.
- [77] Matteo Cococcioni and Stefano De Gironcoli. Linear response approach to the calculation of the effective interaction parameters in the $\text{Lda}+u$ method. *Physical Review B*, 71(3):035105, 2005.
- [78] F Aryasetiawan, M Imada, A Georges, G Kotliar, S Biermann, and AI Lichtenstein. Frequency-dependent local interactions and low-energy effective models from electronic structure calculations. *Physical Review B*, 70(19):195104, 2004.
- [79] Nicola Marzari and David Vanderbilt. Maximally localized generalized wannier functions for composite energy bands. *Physical review B*, 56(20):12847, 1997.
- [80] Ivo Souza, Nicola Marzari, and David Vanderbilt. Maximally localized wannier functions for entangled energy bands. *Physical Review B*, 65(3):035109, 2001.
- [81] Nicola Marzari, Arash A Mostofi, Jonathan R Yates, Ivo Souza, and David Vanderbilt. Maximally localized wannier functions: Theory and applications. *Reviews of Modern Physics*, 84(4):1419, 2012.
- [82] Takashi Miyake and F Aryasetiawan. Screened coulomb interaction in the maximally localized wannier basis. *Physical Review B*, 77(8):085122, 2008.
- [83] Kazuma Nakamura, Ryotaro Arita, and Masatoshi Imada. Ab initio derivation of low-energy model for iron-based superconductors lafeaso and lafepo . *Journal of the Physical Society of Japan*, 77(9):093711, 2008.
- [84] Takashi Miyake, Ferdi Aryasetiawan, and Masatoshi Imada. Ab initio procedure for constructing effective models of correlated materials with entangled band structure. *Physical Review B*, 80(15):155134, 2009.
- [85] Takashi Miyake, Kazuma Nakamura, Ryotaro Arita, and Masatoshi Imada. Comparison of ab initio low-energy models for lafepo , lafeaso , bafes2as2 , lifeso , feso , and fete : electron correlation and covalency. *Journal of the Physical Society of Japan*, 79(4):044705, 2010.
- [86] A Georges, G Kotliar, W Krauth, and M J Rozenberg. Dynamical mean-field theory of strongly correlated fermion systems and the limit of infinite dimensions. *Reviews of Modern Physics*, 68(1):13–125, January 1996.
- [87] Philipp Werner, Armin Comanac, Luca de’ Medici, Matthias Troyer, and Andrew Millis. Continuous-Time Solver for Quantum Impurity Models. *Physical Review Letters*, 97(7):076405, August 2006.
- [88] Philipp Werner and Andrew Millis. Hybridization expansion impurity solver: General formulation and application to Kondo lattice and two-orbital models. *Physical Review B*, 74(15):155107, October 2006.
- [89] Hiroshi Shinaoka, Emanuel Gull, and Philipp Werner. Continuous-time hybridization expansion quantum impurity solver for multi-orbital systems with complex hybridizations. *Computer Physics Communications*, 215:128–136, June 2017.
- [90] Runzhi Wang, Ara Go, and Andrew J Millis. Electron interactions, spin-orbit coupling, and intersite correlations in pyrochlore iridates. *Physical Review B*, 95(4):045133, January 2017.

- [91] Hishiro T Hirose, Jun-ichi Yamaura, and Zenji Hiroi. Robust ferromagnetism carried by antiferromagnetic domain walls. *Scientific Reports*, 7:42440, February 2017.
- [92] T C Fujita, Y Kozuka, M Uchida, A Tsukazaki, T Arima, and M Kawasaki. Odd-parity magnetoresistance in pyrochlore iridate thin films with broken time-reversal symmetry. *Scientific Reports*, 5:9711, May 2015.
- [93] T C Fujita, M Uchida, Y Kozuka, S Ogawa, A Tsukazaki, T Arima, and M Kawasaki. All-in-all-out magnetic domain size in pyrochlore iridate thin films as probed by local magnetotransport. *Applied Physics Letters*, 108(2):022402, 2016.
- [94] E Y Ma, Y T Cui, K Ueda, S Tang, K Chen, N Tamura, P M Wu, J Fujioka, Y Tokura, and Z X Shen. Mobile metallic domain walls in an all-in-all-out magnetic insulator. *Science*, 350(6260):538–541, October 2015.
- [95] Youhei Yamaji and Masatoshi Imada. Metallic Interface Emerging at Magnetic Domain Wall of Antiferromagnetic Insulator: Fate of Extinct Weyl Electrons. *Physical Review X*, 4(2):021035, May 2014.
- [96] Youhei Yamaji and Masatoshi Imada. Modulated helical metals at magnetic domain walls of pyrochlore iridium oxides. *Physical Review B*, 93(1):195146, May 2016.
- [97] Xiang Hu, Zhicheng Zhong, and Gregory A Fiete. First Principles Prediction of Topological Phases in Thin Films of Pyrochlore Iridates. *Scientific Reports*, 5(1):11072, June 2015.
- [98] Bohm-Jung Yang and Naoto Nagaosa. Emergent Topological Phenomena in Thin Films of Pyrochlore Iridates. *Physical Review Letters*, 112(24):246402–5, June 2014.
- [99] H Sakai, K Yoshimura, H Ohno, H Kato, S Kambe, R E Walstedt, T D Matsuda, and Y Haga. Superconductivity in a pyrochlore oxide, Cd₂Re₂O₇. *Journal of Physics: Condensed Matter*, 13(33):L785–L790, 2001.
- [100] H Sakai, H Ohno, K Yoshimura, H Kato, S Kambe, R E Walstedt, T D Matsuda, Y Haga, S Ikeda, and Y Onuki. Superconductivity in pyrochlore oxide Cd₂Re₂O₇. *Physica C-Superconductivity and Its Applications*, 378-381:43, 2002.
- [101] M Hanawa, Y Muraoka, T Tayama, T Sakakibara, J Yamaura, and Z Hiroi. Superconductivity at 1 K in Cd₂Re₂O₇. *Physical Review Letters*, 87:187001, October 2001.
- [102] Jun-ichi Yamaura and Zenji Hiroi. Low Temperature Symmetry of Pyrochlore Oxide Cd₂Re₂O₇. *Journal of the Physical Society of Japan*, 71(11):2598–2600, June 2002.
- [103] J P Castellan, B D Gaulin, J van Duijn, M J Lewis, M D Lumsden, R Jin, J He, S E Nagler, and D Mandrus. Structural Ordering and Symmetry Breaking in Cd₂Re₂O₇. *Physical Review B*, 66:134528, October 2002.
- [104] Mark T Weller, Robert W Hughes, Joanna Rooke, Christopher S Knee, and Jon Reading. The pyrochlore family ? a potential panacea for the frustrated perovskite chemist. *Dalton Transactions*, (19):3032, 2004.
- [105] I A Sergienko, V Keppens, M McGuire, R Jin, J He, S H Curnoe, B C Sales, P Blaha, D J Singh, K Schwarz, and D Mandrus. Metallic “Ferroelectricity” in the Pyrochlore Cd₂Re₂O₇. *Physical Review Letters*, 92(6):065501, February 2004.
- [106] C A Kendziora, I A Sergienko, R Jin, J He, V Keppens, B C Sales, and D Mandrus. Goldstone-Mode Phonon Dynamics in the Pyrochlore Cd₂Re₂O₇. *Physical Review Letters*, 95(12):125503, September 2005.
- [107] Jesse C Petersen, Michael D Caswell, J Steven Dodge, Ivan A Sergienko, Jian He, Rongying Jin, and David Mandrus. Nonlinear optical signatures of the tensor order in Cd₂Re₂O₇. *Nature Physics*, 2(9):605–608, August 2006.
- [108] J W Harter, Z Y Zhao, J Q Yan, D G Mandrus, and D Hsieh. A parity-breaking electronic nematic phase transition in the spin-orbit coupled metal Cd₂Re₂O₇. *Science*, 356(6):295–299, April 2017.
- [109] J W Harter, D M Kennes, H Chu, A de la Torre, Z Y Zhao, J Q Yan, D G Mandrus, A J Millis, and D Hsieh. Evidence of an Improper Displacive Phase Transition in Cd₂Re₂O₇ via Time-Resolved Coherent Phonon Spectroscopy. *Physical Review Letters*, 120(4):047601, January 2018.
- [110] Zenji Hiroi, Jun-ichi Yamaura, Tatsuo C Kobayashi, Yasuhito Matsubayashi, and Daigorou Hirai. Pyrochlore Oxide Superconductor Cd₂Re₂O₇ Revisited. *Journal of the Physical Society of Japan*, 87(2):024702, February 2018.
- [111] O Vyaselev, K Arai, K Kobayashi, J Yamazaki, K Kodama, M Takigawa, M Hanawa, and Z Hiroi. Superconductivity and Magnetic Fluctuations in Cd₂Re₂O₇ via Cd Nuclear Magnetic Resonance and Re Nuclear Quadrupole Resonance. *Physical Review Letters*, 89(1):017001, June 2002.
- [112] Zenji Hiroi, Masafumi Hanawa, Yuji Muraoka, and Hisatomo Harima. Correlations and Semimetallic Behaviors in Pyrochlore Oxide Cd₂Re₂O₇. *Journal of the Physical Society of Japan*, 72(1):21–24, January 2003.
- [113] Liang Fu. Parity-Breaking Phases of Spin-Orbit-Coupled Metals with Gyrotropic, Ferroelectric, and Multipolar Orders. *Physical Review Letters*, 115(2):026401, July 2015.
- [114] J Yamaura, K Takeda, Y Ikeda, N Hirao, Y Ohishi, T C Kobayashi, and Z Hiroi. Successive spatial symmetry breaking under high pressure in the spin-orbit-coupled metal Cd₂Re₂O₇. *Physical Review B*, 95:020102(R), 2017.